CASE REPORT

Intraductal Oncocytic Papillary Neoplasm of the Pancreas: A Radio-Pathological Case Study

Michael A Fischer[1], Olivio Donati[1], Stefan Heinrich[2], Achim Weber[3], Thomas F Hany[4], Davide Soldini[3], Hatem Alkadhi[1], Borut Marincek[1], Hans Scheffel[1]

[1]Institute of Diagnostic Radiology; [2]Clinic of Visceral and Transplant Surgery; [3]Institute of Surgical Pathology; [4]Clinic of Nuclear Medicine; University Hospital Zurich. Zurich, Switzerland

ABSTRACT

Context An intraductal oncocytic papillary neoplasm is a rare pancreatic tumor with the potential of developing invasive carcinoma. Its differentiation from other cystic-like neoplasms of the pancreas, such as intraductal papillary mucinous neoplasms, is a challenge for pancreatic imaging. **Case report** We present the case of a 76-year-old male with painless jaundice caused by an intraductal oncocytic papillary neoplasm of the pancreas. The imaging findings on computed tomography, magnetic resonance including diffusion-weighted imaging, and ^{18}F-fluorodeoxyglucose positron emission tomography are presented and the radio-pathological correlations are discussed. **Conclusion** An intraductal oncocytic papillary neoplasm of the pancreas appears as a cystic tumor communicating with the dilated pancreatic duct featuring intraductal tumor nodules. Intraductal oncocytic papillary neoplasms show a high ^{18}F-fluorodeoxyglucose-uptake in positron emission tomography and low diffusion values in diffusion-weighted imaging including apparent diffusion coefficient maps which may be a valuable attribute in distinguishing these rare lesions from intraductal papillary mucinous neoplasms.

INTRODUCTION

An intraductal oncocytic papillary neoplasm is a rare pancreatic tumor which was first described by Adsay *et al*. in 1996 [1]. Until now, only a few case reports and small series have been reported in the literature [1, 2, 3, 4, 5, 6, 7, 8, 9, 10]. An intraductal oncocytic papillary neoplasm is a distinct entity, having the potential of developing invasive carcinoma, and must be differentiated from other cystic-like neoplasms of the pancreas, such as intraductal papillary mucinous neoplasms (IPMNs) [2]. Both intraductal oncocytic papillary neoplasms and IPMNs appear cystic because they cause ductal dilation due to the intraductal proliferation of mucinous cells [4]. The formation of the tumor cells of intraductal oncocytic papillary neoplasm (such as oncocytic cells and the complex morphology of the papillae) distinguishes them from the more common IPMN [1]. However, the clinical and pathological details of intraductal oncocytic papillary neoplasms remain unclear and are still under debate [5]; some authors have argued that intraductal oncocytic papillary neoplasms are a subgroup of IPMNs [1]. However, the latest classification separates both entities [11].

We performed computed tomography (CT) and magnetic resonance imaging (MRI) as well as diffusion-weighted imaging and ^{18}F-fluorodeoxyglucose positron emission tomography (FDG-PET) on a patient with an intraductal oncocytic papillary neoplasm. The images obtained and the radio-pathological correlations are discussed.

Received October 7th, 2009 - Accepted November 5th, 2009

Key words Carcinoma, Pancreatic Ductal; Diffusion Magnetic Resonance Imaging; Fluorodeoxyglucose F18; Magnetic Resonance Imaging; Pancreas; Positron-Emission Tomography; Tomography, X-Ray Computed

Correspondence Hans Scheffel
Institute of Diagnostic Radiology, University Hospital Zurich, Raemistr. 100, 8091 Zurich, Switzerland
Phone: +41-(0)44.255.3059; Fax: +41-(0)44.255.4506
E-mail: hans.scheffel@usz.ch

URL http://www.jop.unina.it/index.php/jop/article/view/3871/4313

CASE REPORT

A 76-year-old male underwent ultrasonography of the abdomen due to painless jaundice. A cystic tumor in the pancreatic head was discovered and the patient was admitted to our hospital for further evaluation and treatment. Physical examination revealed scleral icterus but was otherwise normal. He suffered from pre-existing arterial hypertension and actinic keratodermia of the vertex. Routine laboratory tests on admission showed elevated serum concentrations of the liver and pancreatic enzymes (AST 215 U/L, reference range 10-50 U/L; ALT 288 U/L, reference range 10-50 U/L; GGT 860 U/L, reference range 8-61 U/L; alkaline phosphatase 599 U/L, reference range 40-129 U/L; pancreatic amylase 130 U/L, reference range 13-53

Figure 1. Curved coronal CT image of the pancreas in the portal venous phase of contrast enhancement. Communication of the mainly cystic intraductal oncocytic papillary neoplasm to the main pancreatic duct in the pancreatic head (arrowhead) and tail is clearly depicted (arrows). Please note the considerable size of the solid tumor part in the tail of the pancreas (asterisk).

U/L) as well as elevated serum bilirubin levels (232 µmol/L, reference level: 0-21 µmol/L). The tumor marker, CA 19-9, was within normal limits.

Imaging Findings

CT (Somatom Definition, Siemens Medical Solutions, Forchheim, Germany) confirmed the cystic lesion in the pancreatic head and revealed another cystic lesion in the pancreatic tail. Both lesions contained several septae and solid elements which showed uptake of iodine-containing contrast media (Figure 1). The main pancreatic duct was dilated in the pancreatic head, body, and tail. Furthermore, dilatation of the common bile duct as well as of the intrahepatic bile ducts was found.

MRI (Signa EchoSpeed EXCITE HD, 1.5 Tesla, GE Healthcare, Waukesha, WI, U.S.A.) was performed and showed two mainly cystic tumors in the pancreatic head and tail with low intensity in T1-weighted images and high intensity in T2-weighted images. The intracystic solid tumor nodules were T1 and T2 hypointense and showed an intensive early, focal gadolinium uptake on dynamic contrast-enhanced T1-weighted images (Figure 2ab). T1-weighted contrast-enhanced images, T2-weighted images, and magnetic resonance cholangiopancreatography (MRCP) clearly depicted the communication between the two separate tumors and the pancreatic duct (Figure 2c).

Diffusion-weighted imaging was performed using a diffusion-weighted single-shot echo-planar-imaging sequence with short tau inversion recovery-based fat-suppression. This diffusion-weighted imaging sequence was performed under breath-hold during inspiration. Water diffusion was measured at b-values of 0, 150, 500, and 1,000 s/mm^2. Diffusion-weighted imaging visualized the solid tumor parts, the pancreatic duct and the distal common bile duct as well as the cystic parts in the pancreatic head and tail with different intensities up to the b-value used. The signal intensities of all the cystic tumor parts were the highest on diffusion-weighted imaging with lower b-factors. At a higher b-factor (b=500 s/mm^2), the signal intensities of the cysts decreased considerably, suggesting a T2 shine-through effect. Apparent diffusion coefficient maps confirmed these findings with high values ($0.97x10^{-3}$ mm^2/s) for all the cystic lesions and low values ($0.57x10^{-3}$ mm^2/s) for the solid tumor parts within the cysts as well as in the pancreatic duct ($0.62x10^{-3}$ mm^2/s) (Figure 3).

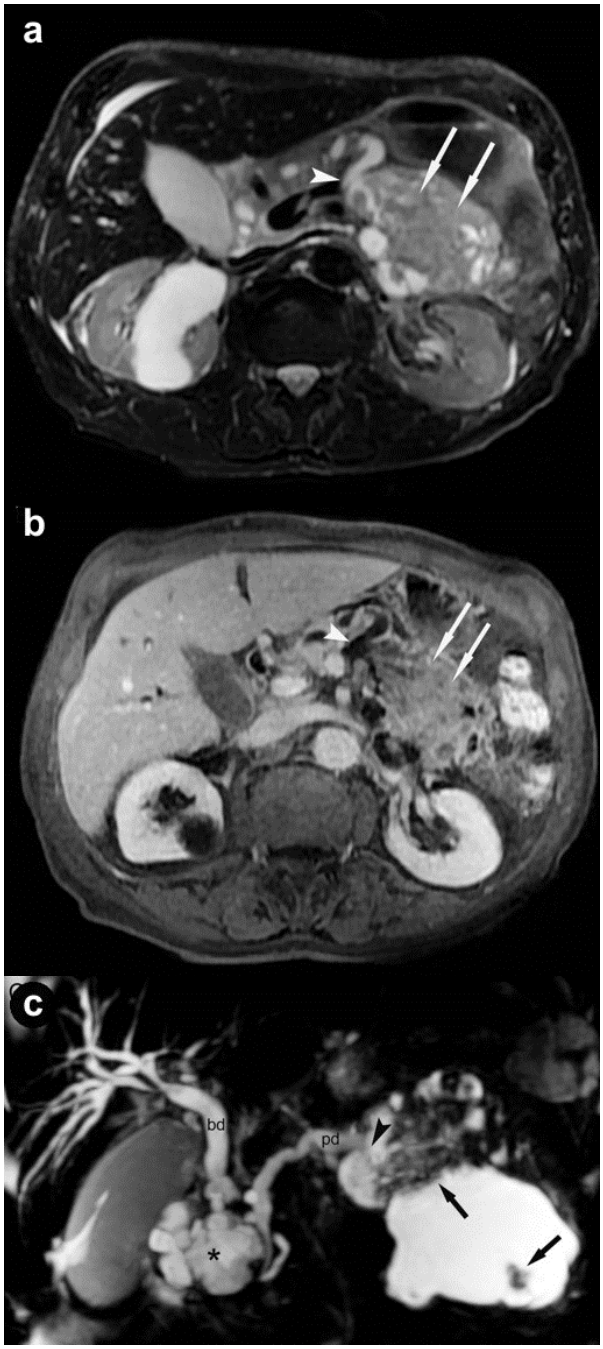

Figure 2. a. Axial T2-weighted image at the level of the pancreas shows the manifestation of the intraductal oncocytic papillary neoplasm in the pancreatic tail. Communication to the pancreatic duct can be identified (arrowhead) as well as the hypointense solid tumor parts (arrows). **b.** Axial T1-weighted image after contrast enhancement with gadolinium at the same level also shows communication to the pancreatic duct and strong enhancement of the solid tumor parts (arrows). **c.** MRCP clearly depicts communication of the dilated pancreatic duct (pd) with the intraductal oncocytic papillary neoplasm in the pancreatic head (asterisk) and tail (arrowhead); the solid tumor components are observable. (bd: dilated common bile duct).

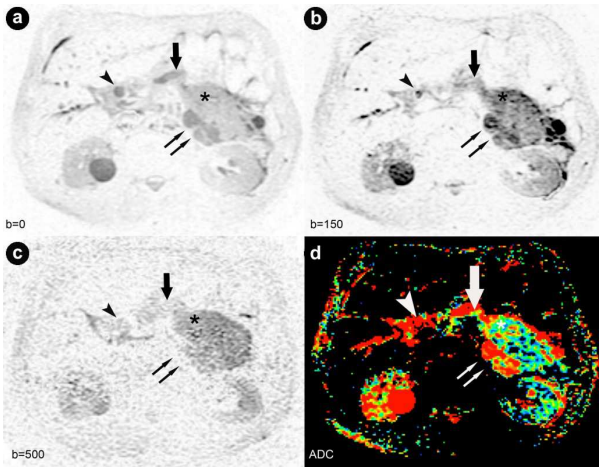

Figure 3. Diffusion weighted images at b=0, 150 and 500 s/mm^2 and apparent diffusion coefficient-mapping generated from b-values at b=150 s/mm^2. **a. b. c.** Axial diffusion-weighted images displayed with an inverted grey-scale at the level of the pancreatic tail acquired at b=0, 150 and 500 s/mm^2. The diffusion-weighted imaging sequences allowed the visualization of the solid tumor parts (asterisk), the pancreatic duct (arrow), the distal common bile duct (arrowhead) as well as the cystic parts in the pancreatic tail (double arrow) with different intensity. Signal intensities of all the cystic tumor parts were highest on diffusion-weighted imaging with b-values at 0 and 150 s/mm^2; with a higher b-value of 500 s/mm^2, signal intensities of the cysts decreased significantly indicating a T2 shine through effect. **d.** Apparent diffusion coefficient-maps confirmed the T2 shine-through effect for all cystic lesions (colored red; double arrow) but not for the solid tumor parts within the cystic components and the pancreatic duct (colored blue; asterisk and arrow). Intraductal oncocytic papillary neoplasm in the common bile duct, confirmed pathologically, was not identifiable on apparent diffusion coefficient-mapping (arrowhead).

FDG-PET acquired on a combined PET-CT in-line system (Discovery VCT; GE HealthCare, Waukesha, WI, U.S.A.) showed an increased uptake by the intracystic solid tumor parts in the pancreatic head (standard uptake value, SUV: 15.4) and tail (SUV: 17.8), consistent with high metabolic activity (Figure 4).

Surgical Findings

Due to the multilocular spread of the pancreatic tumor, a total splenopancreatectomy with partial resection of the stomach, duodenum and omentum was considered necessary; this was successfully performed after diagnostic laparoscopy which ruled out peritoneal implants. The tumor was well encapsulated without signs of vascular infiltration. Interestingly, the common bile duct had to be resected several times due to intra-ductal papillary proliferations in the fresh frozen sections. The reconstruction included an end-to-side hepatojejunostomy as well as an end-to-side gastrojejunostomy with Braun's anastomosis. The patient was discharged for further rehabilitation after an uneventful postoperative course of 15 days.

Pathological Findings

The surgical specimen contained a 10 cm multilocular cystic mass with several papillary projections in the tail of the pancreas and a 6 cm solid area in the head of the

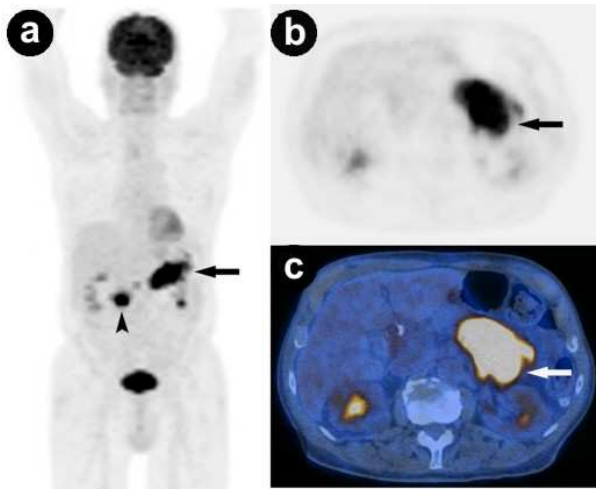

Figure 4 a. Original attenuation-corrected coronal PET image demonstrates high uptake in the pancreatic head (arrowhead) and tail (arrow). **b. c.** Original attenuation-corrected axial PET image at the level of the pancreas shows high uptake in the pancreatic tail (arrow). Corresponding fused FDG-PET/CT at the same level.

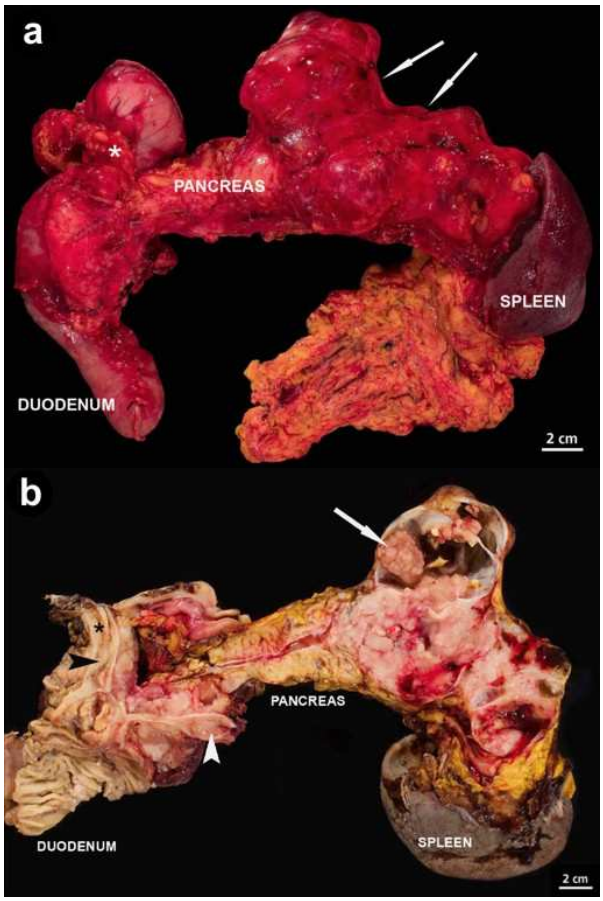

Figure 5. a. Surgical specimen composed of partial gastrectomy, duodenum, pancreas, spleen, and partial omentum. The pancreas is enlarged and shows nodular formations, mainly located in the tail (arrows). (asterisk: ductus choledochus). **b.** Cut surface of the pancreas, revealing a solid area in the head of the pancreas and a multilocular lesion in the tail of the pancreas with solid and cystic parts which contain slightly thick mucin and soft grey-brown luminal papillary masses (arrow). One of these papillary masses is also present in the ductus choledochus (arrowhead), close to the surgical resection margin (asterisk). Ductus choledochus and main pancreatic duct appear dilated.

pancreas which caused dilatation of the main pancreatic duct (Figure 5). Microscopic features of the pancreatic tumor showed a particularly complex architecture with arborizing papillae as well as invasive areas characterized by small nests of cells with extracellular mucin accumulation. The tumor cells in both components showed abundant granular eosinophilic cytoplasm, a characteristic feature of this neoplasm due to numerous mitochondria (Figure 6).
The neoplastic cells expressed abundant and diffuse hepatocyte paraffin-1 and cytokeratin 19 whereas the expression of CEA, MUC1, MUC2 and synaptophysin was focal. No expression of CDX2 or chromogranin was observed.
Of the 21 regional lymph nodes examined, we found a metastatic process in only two of them.

DISCUSSION

Up to now, to the best of our knowledge, only 20 cases of patients having an intraductal oncocytic papillary neoplasm of the pancreas have been reported in the literature [1, 2, 3, 4, 5, 6, 7, 8, 9, 10] and only seven of them involved MRI and CT imaging [2, 3, 4, 5, 6, 7, 8]. All these cases showed almost similar imaging findings describing a cystic tumor with dilatation of the pancreatic duct and nodule-like intraductal tumor parts with uptake of iodine or gadolinium-containing contrast media. Four cases, like ours, showed multilocular tumor involvement [2, 4, 6, 7] whereas the other cases were monolocular [3, 8]. Three cases had metastatic involvement of the liver [1, 7, 10] and one case had regional lymph node metastases [3]. These findings are consistent with the images obtained in our case where no distant metastases were present but there was regional lymph node involvement which was solely detected pathologically and not by CT, MRI, diffusion-weighted imaging or FDG-PET. In all cases reported, a preoperative differentiation of intraductal oncocytic papillary neoplasms from IPMNs could not be made using MRI and CT. Except for one case, where the intraductal oncocytic papillary neoplasm showed no communication with the main pancreatic duct and, therefore, mimicked a mucinous cystic neoplasm [5], communication with the main pancreatic duct was the leading feature for the assumed diagnosis of an IPMN. MRCP is still the best non-invasive imaging modality for IPMNs, being superior to endoscopic retrograde cholangiopancreatography (ERCP) in the detection of cystic dilatation of the pancreatic ducts, number of nodules or septa in the dilated branch duct, as well as demonstrating communication of cystic tumors with the main pancreatic duct [12]. In our case, MRI and MRCP clearly depicted the communication of the intraductal oncocytic papillary neoplasm to the main pancreatic duct. We were also able to detect nodule-like intraductal tumor parts on MRCP and its source images.
FDG-PET has proved to be useful for detecting malignant tumors of the pancreas, distant metastases in suspected pancreatic cancer, and parenchymal invasion of IPMN [13, 14]. Sperti *et al*. recently reported that ^{18}F-FDG PET was more accurate than MRI and CT in distinguishing benign from malignant IPMNs [15]. Experience with intraductal oncocytic papillary neoplasm is limited, with only two case reports until now [4, 8]. Both cases showed strong FDG-uptake of the tumor nodules within the cystic components, with standard uptake values (SUVs) comparable to our case. Generally, benign tumors show significantly lower SUVs as compared to malignant tumors indicating a lower glucose-metabolism, which correlates with the diminished biological activity. The SUVs in the present case were very high. One reasonable explanation might be that intraductal oncocytic papillary neoplasms have high replication rates and therefore a higher glucose-metabolism. Oncocytomas have generally been proven to be notably active metabolically. As a matter of fact, several cases of non-pancreatic oncocytoma including those in the thyroid, pararenal, submandibular, and parotid glands showed intense activity on ^{18}F-FDG-PET [16, 17, 18, 19]. In our case, the intraductal oncocytic papillary neoplasm was not solely intraepithelial since histological evaluation revealed multilocular transformation to invasive carcinoma which may have also caused high SUVs. However, in both published cases involving FDG-PET and intraductal oncocytic papillary neoplasms, there was no evidence of tumor invasion but there was still notable metabolic activity [4, 8].
Diffusion-weighted imaging has proven to be feasible for tumor and metastasis detection in a whole-body setting [20]. Diffusion-weighted imaging was shown to be useful in the detection and characterization of malignant hepatic lesions [21] and pancreatic cancer [22]. Whereas small b-values (b=20-50 s/mm^2) are considered to give the best results in tumor detection of the liver [21], in pancreatic tumor imaging higher b-

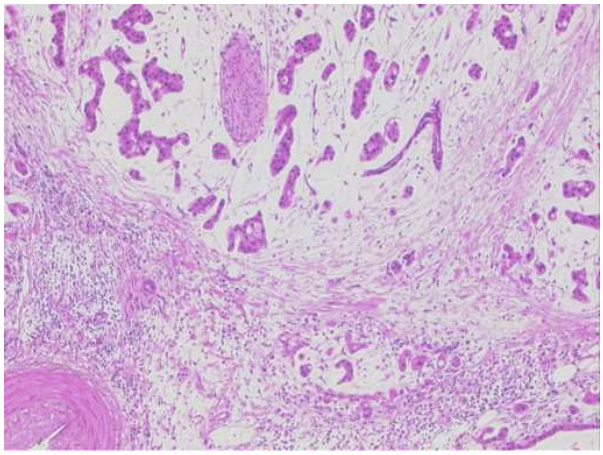

Figure 6. Microscopic features of the pancreatic tumor showing a particularly complex architecture with arborizing papillae as well as invasive areas characterized by small nests of cells with extracellular mucin accumulation. Invasion front composed of tumor cells with abundant eosinophilic cytoplasm surrounded by abundant mucin. A perineural invasion in the tumor area can also be observed as can a peritumoral desmoplastic stromal reaction.

values (b=1,000 s/mm^2) have added diagnostic value [23].

In the present case, diffusion-weighted imaging with low and medium b-values (b=150, 500 s/mm^2) allowed a clear depiction and differentiation of the solid and cystic tumor parts as compared to the regular pancreatic tissue. The solid tumor parts mostly represent the papillary component of the intraductal oncocytic papillary neoplasm which was also detectable by MRI and CT. This correlated very well with the macropathologic specimen after a total pancreatectomy. In contrast to FDG-PET, we also found low diffusion values in the main pancreatic duct and the distal common bile duct. Yamashita *et al*. found restricted perfusion in mucine-containing pancreatic cysts as compared to cysts of other origins at a b-value of 300 s/mm^2 [24]. Thus, our findings indicate mucin or papillary tumor components filling the pancreatic duct system and the distal common bile duct. This is the first intraductal oncocytic papillary neoplasm case study which includes diffusion-weighted imaging. Only one recent study evaluated diffusion-weighted imaging in IPMNs and showed no restricted diffusion, indicating its feasibility in differentiating these two entities [25].

All cystic tumor parts as well as the coexisting right-sided kidney cysts showed higher intensity on diffusion-weighted imaging (b=150 s/mm^2) as compared to the solid tumor nodules, with slightly less intensity on b=500 s/mm^2, indicating a strong T2 shine-through effect. Apparent diffusion coefficient maps confirmed the T2 shine-through effect by showing high values for all cystic parts and low values for the solid tumor part [26]. In a recent study, significant differences between the signal intensity ratios of pancreatic cystic lesions were found on images at a b factor of 1,000 s/mm^2, making the differentiation of pancreatic cysts possible [27]. However, with a higher b factor (b =1,000 s/mm^2), we obtained a very low signal-to-noise ratio causing anatomic distortion due to susceptibility effects which did not allow diagnostic image interpretation. This is a well-known problem for echo-planar sequences with higher b-values resulting in greater image distortion [28].

The clinical significance of preoperative differentiation of intraductal oncocytic papillary neoplasms from IPMNs can only be estimated at this point because the degree of malignant potential for intraductal oncocytic papillary neoplasms is still unclear due to the low number of cases reported. Standard surgical therapeutic intervention for both lesions is a pylorus-preserving pancreaticoduodenectomy, as was carried out in our case. However, the majority of the intraductal oncocytic papillary neoplasm cases reported in the literature were diagnosed as carcinomas including reports of invasive tumor growth and distant metastasis which changes the surgical procedure to extended pancreatectomy. In contrast, only one of these cases involved death from an intraductal oncocytic papillary neoplasm; good prognoses can be expected but short follow-up periods are indicated.

CONCLUSION

Intraductal oncocytic papillary neoplasms of the pancreas should be included in the differential diagnosis of cystic tumors with communication to the dilated pancreatic duct featuring intraductal tumor nodules. An intraductal oncocytic papillary neoplasm shows a high FDG uptake in PET and low diffusion values in diffusion-weighted imaging, including apparent diffusion coefficient maps which may be a valuable attribute in distinguishing these rare lesions from IPMNs.

Conflict of interest The authors have no potential conflicts of interest

References

1. Adsay NV, Adair CF, Heffess CS, Klimstra DS. Intraductal oncocytic papillary neoplasms of the pancreas. Am J Surg Pathol 1996; 20:980-94. [PMID 8712298]

2. Jyotheeswaran S, Zotalis G, Penmetsa P, Levea CM, Schoeniger LO, Shah AN. A newly recognized entity: intraductal "oncocytic" papillary neoplasm of the pancreas. Am J Gastroenterol 1998; 93:2539-43. [PMID 9860422]

3. Nobukawa B, Suda K, Suyama M, Ariyama J, Beppu T, Futagawa S. Intraductal oncocytic papillary carcinoma with invasion arising from the accessory pancreatic duct. Gastrointest Endosc 1999; 50:864-6. [PMID 10570358]

4. Noji T, Kondo S, Hirano S, Ambo Y, Tanaka E, Katoh C, et al. Intraductal oncocytic papillary neoplasm of the pancreas shows strong positivity on FDG-PET. Int J Gastrointest Cancer 2002; 32:43-6. [PMID 12630769]

5. Oku T, Maeda M, Wada Y, Waga E, Ono K, Nagamachi Y, et al. Intraductal oncocytic papillary neoplasm having clinical characteristics of mucinous cystic neoplasm and a benign histology. JOP. J Pancreas (Online) 2007; 8:206-13. [PMID 17356245]

6. Shima Y, Yagi T, Inagaki M, Sadamori H, Tanaka N, Horimi T, et al. Intraductal oncocytic papillary neoplasm of the pancreas with celiac artery compression syndrome and a jejunal artery aneurysm: report of a case. Surg Today 2005; 35:86-90. [PMID 15622472]

7. Thompson K, Castelli MJ, Gattuso P. Metastatic papillary oncocytic carcinoma of the pancreas to the liver diagnosed by fine-needle aspiration. Diagn Cytopathol 1998; 18:291-6. [PMID 9557266]

8. Kato Y, Nakagouri T, Konishi M, Takahashi S, Gotoda N, Hasebe T, Kinosita T. Intraductal oncocytic papillary neoplasm of the pancreas with strong accumulation on FDG-PET. Hepatogastroenterology 2008; 55:900-2. [PMID 18705293]

9. Ishida M, Egawa S, Aoki T, Sakata N, Mikami Y, Motoi F, et al. Characteristic clinicopathological features of the types of intraductal papillary-mucinous neoplasms of the pancreas. Pancreas 2007; 35:348-52. [PMID 18090241]

10. Patel SA, Adams R, Goldstein M, Moskaluk CA. Genetic analysis of invasive carcinoma arising in intraductal oncocytic papillary neoplasm of the pancreas. Am J Surg Pathol 2002; 26:1071-7. [PMID 12170096]

11. Hruban R, Pitman MB, Klimstra DS. AFIP Atlas of Tumor Pathology. Tumors of the Pancreas. Series 4, Fasc 6: Washington, American Registry of Pathology in collaboration with Armed Forces Institute of Pathology, 2007, pp 23-50.

12. Itai Y, Minami M. Intraductal papillary-mucinous tumor and mucinous cystic neoplasm: CT and MR findings. Int J Gastrointest Cancer 2001; 30:47-63. [PMID 12489580]

13. Strobel K, Heinrich S, Bhure U, Soyka J, Veit-Haibach P, Pestalozzi BC, et al. Contrast-enhanced 18F-FDG PET/CT: 1-stop-shop imaging for assessing the resectability of pancreatic cancer. J Nucl Med 2008; 49:1408-13. [PMID 18703604]

14. Yoshioka M, Sato T, Furuya T, Shibata S, Andoh H, Asanuma Y, et al. Positron emission tomography with 2-deoxy-2-[(18)F] fluoro- d-glucose for diagnosis of intraductal papillary mucinous tumor of the pancreas with parenchymal invasion. J Gastroenterol 2003; 38:1189-93. [PMID 14714260]

15. Sperti C, Bissoli S, Pasquali C, Frison L, Liessi G, Chierichetti F, Pedrazzoli S. 18-fluorodeoxyglucose positron emission tomography enhances computed tomography diagnosis of malignant intraductal papillary mucinous neoplasms of the pancreas. Ann Surg 2007; 246:932-7. [PMID 18043094]

16. Blake MA, McKernan M, Setty B, Fischman AJ, Mueller PR. Renal oncocytoma displaying intense activity on 18F-FDG PET. AJR Am J Roentgenol 2006; 186:269-70. [PMID 16357422]

17. Kim DJ, Chung JJ, Ryu YH, Hong SW, Yu JS, Kim JH. Adrenocortical oncocytoma displaying intense activity on 18F-FDG-PET: a case report and a literature review. Ann Nucl Med 2008; 22:821-8. [PMID 19039562]

18. Subramaniam RM, Durnick DK, Peller PJ. F-18 FDG PET/CT imaging of submandibular gland oncocytoma. Clin Nucl Med 2008; 33:472-4. [PMID 18580232]

19. Hagino K, Tsunoda A, Ishihara A, Kishimoto S, Suzuki T, Hara A. Oncocytoma in the parotid gland presenting a remarkable increase in fluorodeoxyglucose uptake on positron emission tomography. Otolaryngol Head Neck Surg 2006; 134:708-9. [PMID 16564402]

20. Vilanova JC, Barcelo J. Diffusion-weighted whole-body MR screening. Eur J Radiol 2008; 67:440-7. [PMID 18430538]

21. Bruegel M, Rummeny EJ. Hepatic metastases: use of diffusion-weighted echo-planar imaging. Abdom Imaging 2009; May 27. [PMID 19471997]

22. Matsuki M, Inada Y, Nakai G, Tatsugami F, Tanikake M, Narabayashi I, et al. Diffusion-weighted MR imaging of pancreatic carcinoma. Abdom Imaging 2007; 32:481-3. [PMID 17431713]

23. Takeuchi M, Matsuzaki K, Kubo H, Nishitani H. High-b-value diffusion-weighted magnetic resonance imaging of pancreatic cancer and mass-forming chronic pancreatitis: preliminary results. Acta Radiol 2008; 49:383-6. [PMID 18415779]

24. Yamashita Y, Namimoto T, Mitsuzaki K, Urata J, Tsuchigame T, Takahashi M, Ogawa M. Mucin-producing tumor of the pancreas: diagnostic value of diffusion-weighted echo-planar MR imaging. Radiology 1998; 208:605-9. [PMID 9722835]

25. Kartalis N, Lindholm TL, Aspelin P, Permert J, Albiin N. Diffusion-weighted magnetic resonance imaging of pancreas tumours. Eur Radiol 2009; 19:1981-90. [PMID 19308414]

26. Ozsunar Y, Sorensen AG. Diffusion- and perfusion-weighted magnetic resonance imaging in human acute ischemic stroke: technical considerations. Top Magn Reson Imaging 2000; 11:259-272. [PMID 11142625]

27. Inan N, Arslan A, Akansel G, Anik Y, Demirci A. Diffusion-weighted imaging in the differential diagnosis of cystic lesions of the pancreas. AJR Am J Roentgenol 2008; 191:1115-21. [PMID 18806153]

28. Naganawa S, Kawai H, Fukatsu H, Sakurai Y, Aoki I, Miura S, et al. Diffusion-weighted imaging of the liver: technical challenges and prospects for the future. Magn Reson Med Sci 2005; 4:175-186. [PMID 16543702]